energies

Article

Fault-Tolerant Control for Reducing Harmonic Distortion of Dual Three-Phase Permanent Magnet Synchronous Motor

Liping Zhao [1,2], Baojun Ge [1,*], Hanying Gao [1,*] and Dajun Tao [1]

1 School of Electrical and Electronic Engineering, Harbin University of Science and Technology, Harbin 150080, China; zlp@hrbust.edu.cn (L.Z.); taodj@hrbust.edu.cn (D.T.)
2 School of Automation, Harbin University of Science and Technology, Harbin 150080, China
* Correspondence: gebj@hrbust.edu.cn (B.G.); ghy@hrbust.cn (H.G.)

Abstract: Aiming at the open circuit fault of a dual three-phase permanent magnet synchronous motor, a normalized current method is used for open circuit fault diagnosis. Then, a fault-tolerant control strategy for reducing the harmonic distortion of a dual three-phase permanent magnet synchronous motor is proposed, which is based on current model prediction control and keeps the decoupling transformation matrix unchanged. The fault-tolerant control method based on current model prediction considers the influence of the control quantity on the future state of the system, and effectively reduces the total harmonic distortion. Two fault-tolerant control strategies for the motor are analyzed, with minimizing stator copper consumption and maximizing torque output as control objectives. Through simulation and experiment of fault-tolerant control strategies for a dual three-phase permanent magnet synchronous motor, the results verify the effectiveness and feasibility of the strategy.

Keywords: DTP-PMSM; fault tolerant; copper consumption; model prediction

Citation: Zhao, L.; Ge, B.; Gao, H.; Tao, D. Fault-Tolerant Control for Reducing Harmonic Distortion of Dual Three-Phase Permanent Magnet Synchronous Motor. *Energies* **2022**, *15*, 3887. https://doi.org/10.3390/en15113887

Academic Editors: Moussa Boukhnifer, Ahmed Chaibet, Kondo Adjallah and Adolfo Dannier

Received: 10 March 2022
Accepted: 19 April 2022
Published: 25 May 2022

1. Introduction

In recent years, due to the strong reliability, high control freedom and excellent fault tolerance of polyphase motors, they have good application prospects in the case of high power drive [1–4]. The dual three-phase permanent magnet synchronous motor (DTP-PMSM) adopts an asymmetric six phase motor, which is composed of two sets of Y-connected symmetrical three-phase windings with phase shifts of a 30° electrical angle. The neutral points of the two sets of windings can be divided into a single neutral point and a neutral point isolation connection mode. Neutral point isolation is more commonly used in DTP-PMSM, as the neutral point isolation connection mode can effectively inhibit the zero-sequence current [5–7].

When a phase open circuit fault occurs, the most simple and intuitive method is to cut off the fault set of the three-phase windings, and turn it into an ordinary three-phase motor. However, it cannot take full advantage of the redundancy of the multiphase motor, which results in wasting of resources. Therefore, a good fault-tolerant control strategy is the key to give full play to the superior fault-tolerant performance of the polyphase motor.

In [8], the neutral point of the three-phase PMSM was connected to the midpoint of two split capacitors by means of a triode for an alternating current to keep the continual operation when open-phase faults occur. A fault-tolerant control method is proposed with the constraints of output smooth torque and reduction of harmonic effect of magnetomotive force in [9]. However, the stator copper loss is not considered, and it is generally realized by current hysteresis control. The current hysteresis method is applied to reallocate the current amplitude and phase outside the fault phase, based on the principle that the magnetomotive force remains unchanged in [10–16]. However, this method requires off-line calculation. It has high dependence on motor parameters, and is not suitable for high-power applications. In [17–25], the reduced order mathematical model of an open phase motor has been established. Due to the strong coupling in the rotating coordinate system, feed-forward control is added to compensate after decoupling. However, the transformation matrix of the mathematical model of an open phase motor is different with different fault phases. In [26], fault-tolerant control of torque mode was proposed in order to consider over-current protection as well as torque capacity. In [27,28], the third harmonic current injection method was used to reduce the torque ripple caused by phase short circuit faults, so the motor can still operate stably in fault. However, this method could produce a harmonic torque problem. A fault-tolerant control strategy of open phase based on normal decoupling transformation matrix was proposed in [29–31], in which a harmonic space current and a zero sequence space current are constructed from a static coordinate current to realize fault-tolerant control. However, in the field-oriented control, it needs to convert the variables to the stationary coordinate system. In [32], it was proposed to add an additional current component to each phase to derive a new current set. In [33], an improved rotating coordinate transformation was proposed to realize vector control of PMSM. However, the above control methods generally use the current hysteresis control, which does not fix the problems of switching frequencies and current harmonics.

In this paper, a fault-tolerant control strategy based on current model prediction control (MPC) is proposed. Differently from the widely existing fault-tolerant control based on a current hysteresis loop or establishing a motor model after a fault, it does not change the motor model, and only changes the harmonic plane and zero sequence plane current from a dq current based on current model prediction, so as to make the motor run stably and effectively reduce the total harmonic distortion (THD) in case of fault. The major contribution is in using the fault-tolerant control method with current model prediction, considering the influence of the control quantity on the future state of the system, which effectively reduces the total harmonic distortion (THD). Two fault-tolerant control strategies for DTP-PMSM are analyzed with minimizing stator copper consumption (MCC) and maximizing torque output (MTO) as control objectives. Through simulation and experiments of fault-tolerant control strategies for DTP-PMSM, the results verify the effectiveness and feasibility of the strategy.

2. Mathematical Model of DTP-PMSM

The DTP-PMSM is composed of two sets of Y-connected three-phase windings with a phase shift of 30°. The winding structure of the motor is shown in Figure 1. The drive system can be divided into single neutral point and neutral point isolation, as shown in Figure 2. A-B-C and D-E-F represent two sets of three-phase windings of DTP-PMSM respectively. The neutral isolation mode is more often used, as it can effectively suppress the zero sequence current.

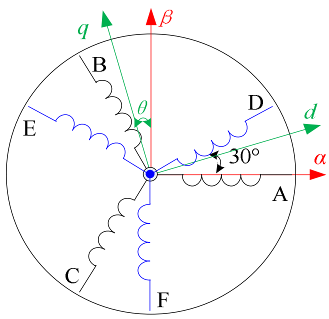

Figure 1. Winding structure of DTP-PMSM.

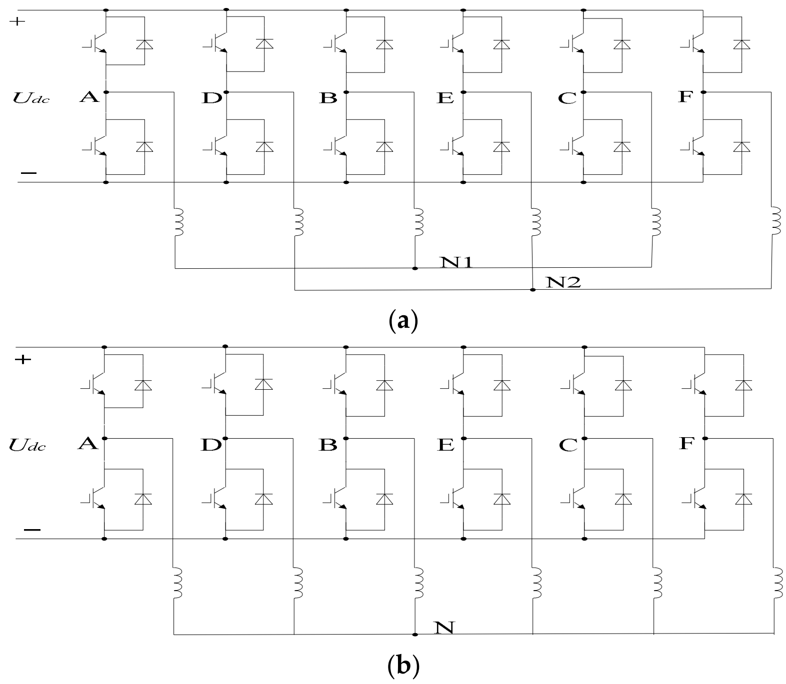

Figure 2. Neutral line connection mode of DTP-PMSM drive system. (**a**) Structure 1. (**b**) Structure 2.

According to the spatial decoupling modeling method, the variables of DTP-PMSM are mapped to the α-β subspace, the z_1-z_2 subspace and the o_1-o_2 zero-sequence subspace. The static transformation can be written as:

$$[\alpha\ \beta]^T = \begin{bmatrix} 1 & -\frac{1}{2} & -\frac{1}{2} & \frac{\sqrt{3}}{2} & -\frac{\sqrt{3}}{2} & 0 \\ 0 & \frac{\sqrt{3}}{2} & -\frac{\sqrt{3}}{2} & \frac{1}{2} & \frac{1}{2} & -1 \end{bmatrix} \cdot [A\ B\ C\ D\ E\ F]^T \tag{1}$$

The relation of each orthogonal vector is:

$$\begin{cases} z_1 \cdot \beta^T = z_1 \cdot \alpha^T = 0 \\ z_2 \cdot {z_1}^T = z_2 \cdot \beta^T = z_2 \cdot \alpha^T = 0 \\ o_1 \cdot {z_2}^T = o_1 \cdot {z_1}^T = o_1 \cdot \beta^T = o_1 \cdot \alpha^T = 0 \\ o_2 \cdot {o_1}^T = o_2 \cdot {z_2}^T = o_2 \cdot {z_1}^T = o_2 \cdot \beta^T = o_2 \cdot \alpha^T = 0 \end{cases} \tag{2}$$

where α-β is the stationary coordinate subspace; z_1-z_2 is the harmonic subspace; o_1-o_2 is the zero-sequence subspace.

Therefore, the unit orthogonal matrix is obtained by transforming the variables of the dual three-phase motor to the static coordinate system. It can be written as:

$$T_{clark} = \frac{1}{3} \begin{bmatrix} 1 & -\frac{1}{2} & -\frac{1}{2} & \frac{\sqrt{3}}{2} & -\frac{\sqrt{3}}{2} & 0 \\ 0 & \frac{\sqrt{3}}{2} & -\frac{\sqrt{3}}{2} & \frac{1}{2} & \frac{1}{2} & -1 \\ 1 & -\frac{1}{2} & -\frac{1}{2} & -\frac{\sqrt{3}}{2} & \frac{\sqrt{3}}{2} & 0 \\ 0 & -\frac{\sqrt{3}}{2} & \frac{\sqrt{3}}{2} & \frac{1}{2} & \frac{1}{2} & -1 \\ 1 & 1 & 1 & 0 & 0 & 0 \\ 0 & 0 & 0 & 1 & 1 & 1 \end{bmatrix} \tag{3}$$

It is necessary to transform α-β components to a synchronous rotation d-q coordinate system. Since the currents in the z_1-z_2 sub-plane and o_1-o_2 sub-plane do not participate in energy conversion, only the α-β sub-plane involved in electromechanical energy conversion needs to be analyzed. Thus, only the α-β sub-plane components are transformed to a rotation reference frame. The rotating transformation matrix is:

$$T_{park} = \begin{bmatrix} \cos\theta & \sin\theta & \mathbf{0} \\ -\sin\theta & \cos\theta & \mathbf{0} \\ \mathbf{0} & \mathbf{0} & \boldsymbol{I_4} \end{bmatrix} \tag{4}$$

where $\boldsymbol{I_4}$ is a four-dimensional unit matrix, and $\mathbf{0}$ is a zero matrix. The final transformation matrix is:

$$T_{6r} = T_{park} \cdot T_{clark} \tag{5}$$

The decoupling voltage equation of the DTP-PMSM in the synchronous rotation coordinate system can be obtained according to (1) and (2). It can be written as:

$$\begin{cases} u_d = R_s i_d + L_d \frac{d}{dt} i_d - \omega_e L_q i_q \\ u_q = R_s i_q + L_q \frac{d}{dt} i_q + (\omega_e L_d i_d + \psi_f) \\ u_{z1} = R_s i_{z1} + L_l \frac{d}{dt} i_{z1} \\ u_{z2} = R_s i_{z2} + L_l \frac{d}{dt} i_{z2} \end{cases} \tag{6}$$

The torque equation is:

$$T_e = 3p_n[(L_d - L_q) i_d i_q + i_q \psi_f] \tag{7}$$

The motion equation is:

$$T_e - T_L - B\omega_m = J\frac{d\omega_m}{dt} \tag{8}$$

where u_d, u_q are voltages in the synchronous rotation coordinate subspace; u_{z1}, u_{z2} are voltages in the harmonic subspace; R_s is the stator resistance; L_d, L_q are the d-q axis main inductance; L_l is leakage inductance; Ψ_f is the flux amplitude generated by the permanent magnet in the winding; ω_e is the rotor electric angular velocity; p_n is the number of motor poles; ω_m is the mechanical angular velocity; J is the moment of inertia; B is the damping coefficient; T_L is the load torque.

3. Open Circuit Fault Diagnosis Based on Normalized Current

The DTP-PMSM has excellent fault-tolerant performance. When the fault occurs, the fault-tolerant control should be carried out to ensure the stable operation of the system. If the fault-tolerant control is not carried out, the fault will worsen and even damage the motor. Thus, it is necessary to diagnose the motor fault in time and start the fault-tolerant control strategy.

A normalized current is used to diagnose the open-circuit faults of DTP-PMSM. Without considering harmonics, the stator current of each phase can be expressed as:

$$\begin{cases} i_A = I_m \cos\theta \\ i_B = I_m \cos(\theta - 120^\circ) \\ i_C = I_m \cos(\theta + 120^\circ) \\ i_D = I_m \cos(\theta - 30^\circ) \\ i_E = I_m \cos(\theta - 150^\circ) \\ i_F = I_m \cos(\theta + 90^\circ) \end{cases} \tag{9}$$

The static coordinate current is obtained by the six-phase current through (3).

$$\begin{cases} i_\alpha = I_m \cos\theta \\ i_\beta = I_m \sin\theta \end{cases} \tag{10}$$

The calculated current vector modulus is as follows:

$$|\vec{i_s}| = \sqrt{i_\alpha^2 + i_\beta^2} = I_m \tag{11}$$

As the stator current of the motor changes with the operating conditions, the normalized calculation is carried out:

$$i_n^* = i_n / |\vec{i_s}| \tag{12}$$

The normalized stator current of each phase is obtained as follows:

$$\begin{cases} i_A^* = i_A / |\vec{i_s}| = \cos\theta \\ i_B^* = i_B / |\vec{i_s}| = \cos(\theta - 120^\circ) \\ i_C^* = i_C / |\vec{i_s}| = \cos(\theta + 120^\circ) \\ i_D^* = i_D / |\vec{i_s}| = \cos(\theta - 30^\circ) \\ i_E^* = i_E / |\vec{i_s}| = \cos(\theta - 150^\circ) \\ i_F^* = i_F / |\vec{i_s}| = \cos(\theta + 90^\circ) \end{cases} \tag{13}$$

The absolute value of the normalized current is averaged, and the expression is as follows:

$$f = \frac{\omega_e}{\pi} \int_0^{\frac{\pi}{\omega_e}} |i_n^*| dt = \frac{2}{\pi}, n = A, B, C, D, E, F \tag{14}$$

where ω_e is the electric angular velocity.

By comparing the calculated value of f with the periodic average value of the absolute value of the actual detected current, the fault characteristic quantity F is obtained, which is expressed as:

$$F = f - Mean(|i_n^*|) \tag{15}$$

When the motor is working normally, the fault characteristic quantity F is approximately 0. If an open circuit fault occurs, the corresponding fault characteristic quantity is f. Thus, it can be determined which phase has an open circuit fault. Then, the corresponding fault-tolerant control starts to ensure the stable operation of the motor.

4. Fault-Tolerant Control Strategy for DTP-PMSM

Model predictive control (MPC) is a control algorithm based on the controlled system model, which can predict the future state of the system and obtain the optimal control of the system by rolling optimization. In order to obtain the dynamic target of finite time domain optimization, the d–q axis current is predicted and optimized as follows:

$$\begin{cases} i_d{}' = (1 - \frac{RT_s}{L_d}) i_d + \frac{\omega_e L_q T_s}{L_d} i_q + \frac{T_s}{L_d} u_d \\ i_q{}' = (1 - \frac{RT_s}{L_q}) i_q - \frac{\omega_e T_s}{L_d} (\psi_f + L_d i_d) + \frac{T_s}{L_q} u_q \end{cases} \tag{16}$$

where T_s is the sampling time.

The predictive control strategy aims to minimize the value function. The value function is:

$$A = (i_d{}' - i_d^*)^2 + (i_q{}' - i_q^*)^2 \tag{17}$$

where id^*, iq^* are the reference currents of the d-q axis.

The fault-tolerant control strategy of DTP-PMSM under two neutral connection modes is studied in the following.

As shown in Figure 2, the current constraint condition in Structure 1 should satisfy the following relation:

$$i_A + i_B + i_C = 0, i_D + i_E + i_F = 0 \tag{18}$$

The current constraint condition in Structure 2 should satisfy the following relation:

$$i_A + i_B + i_C + i_D + i_E + i_F = 0 \tag{19}$$

Assuming the motor is not damaged, and there is an open circuit between the F-phase winding and the inverter, the decoupling transformation matrix remains unchanged as the motor is not affected by physics and only the current will be affected. The dq current, z_1-z_2 harmonic component current and o_1-o_2 zero sequence component current are given for vector control. Since the dq component is related to energy conversion, only the z_1-z_2 and o_1-o_2 plane components are changed for fault-tolerant control in order to leave the output torque unchanged. According to (3) and (4), it is obtained that:

$$i_F = i_d' \cos(\theta + \frac{\pi}{2}) - i_q' \sin(\theta + \frac{\pi}{2}) - i_{z2} + i_{o2} = 0 \tag{20}$$

It can be seen that F-phase current is independent from i_{z1} and i_{o1}.

4.1. Current Optimization Objective with MCC

When minimizing, the stator copper consumption (MCC) is taken as the current optimization goal, and i_{z1} is set to zero since it is independent of the F-phase current. In Structure 1, according to (18), then:

$$i_{o2} = i_{o1} = 0 \tag{21}$$

Thus, we obtain:

$$i_{z2} = -i_d' \sin\theta - i_q' \cos\theta \tag{22}$$

Thus, the harmonic and zero sequence subspace current components can be set as:

$$\begin{cases} i_{z1} = 0 \\ i_{z2} = -i_d' \sin\theta - i_q' \cos\theta \\ i_{o1} = i_{o2} = 0 \end{cases} \tag{23}$$

When the field orientation control method is adopted, then:

$$\begin{cases} i_{z1} = 0 \\ i_{z2} = -i_q' \cos\theta \\ i_{o1} = i_{o2} = 0 \end{cases} \tag{24}$$

Therefore, if i_{z1} is set as zero in the closed loop control, and the zero sequence subspace is set as zero, the control goal can be achieved.

In Structure 2, the dual three-phase motor has a single neutral point. According to (19), then:

$$i_{o1} + i_{o2} = 0 \tag{25}$$

Set the current components of harmonic plane to be:

$$i_{z2} = i_d'\left(k_1 \cos\theta + k_2 \sin\theta\right) + i_q'\left(k_3 \cos\theta + k_4 \sin\theta\right) \tag{26}$$

According to (20) and (25), the zero sequence current can be derived. Since i_{z1} is independent of the F-phase current, it is still given as zero when taking MCC as the goal. In the case of the minimum value of $i_{z1}^2 + i_{z2}^2 + i_{o1}^2 + i_{o2}^2$, then:

$$k_1 = 0, k_2 = -\frac{2}{3}, k_3 = -\frac{2}{3}, k_4 = 0$$

When taking MCC as the goal in Structure 2, the harmonic and zero sequence current components are given as follows:

$$\begin{cases} i_{z1}= 0 \\ i_{z2} = -\frac{2}{3} i_d{}' \sin\theta - \frac{2}{3} i_q{}' \cos\theta \\ i_{o1} = -\frac{1}{3} i_d{}' \sin\theta - \frac{1}{3} i_q{}' \cos\theta \\ i_{o2} = \frac{1}{3} i_d{}' \sin\theta + \frac{1}{3} i_q{}' \cos\theta \end{cases} \tag{27}$$

When the field orientation control method is adopted, $i_d{}' = 0$.

4.2. Current Optimization Objective with MTO

When the maximum torque output (MTO) is taken as the control goal, the maximum output current is guaranteed to be minimized. In Structure 1, $i_{o1} = i_{o2} = 0$. It can be known that i_{z2} remains unchanged according to (18) and (22). Set:

$$i_{z1} = i_d{}'(K_1 \cos\theta + K_2 \sin\theta) + i_q{}'(K_3 \cos\theta + K_4 \sin\theta) \tag{28}$$

Then, the harmonic and zero sequence subspace current components can be set as:

$$\begin{cases} i_{z1} = i_d{}'(K_1 \cos\theta + K_2 \sin\theta) + i_q{}'(K_3 \cos\theta + K_4 \sin\theta) \\ i_{z2} = -i_d{}' \sin\theta - i_q{}' \cos\theta \\ i_{o1} = i_{o2} = 0 \end{cases} \tag{29}$$

According to (3) and (29), each phase current can be expressed by i_d and i_q through the space transformation matrix.

The control objective is to minimize the maximum current amplitude of each phase. Therefore, it is calculated in Structure 1 that:

$$k_1 = -1, k_2= 0, k_3 = 0, k_4 = 1$$

Then, the harmonic and zero sequence subspace components are given as:

$$\begin{cases} i_{z1} = -i_d{}' \cos\theta + i_q{}' \sin\theta \\ i_{z2} = -i_d{}' \sin\theta - i_q{}' \cos\theta \\ i_{o1} = i_{o2} = 0 \end{cases} \tag{30}$$

In field-oriented control, $i_d{}' = 0$.

In Structure 2, set the harmonic plane current components as:

$$\begin{cases} i_{z1} = i_d{}'(k_1 \cos\theta + k_2 \sin\theta) + i_q{}'(k_3 \cos\theta + k_4 \sin\theta) \\ i_{z2} = i_d{}'(k_5 \cos\theta + k_6 \sin\theta) + i_q{}'(k_7 \cos\theta + k_8 \sin\theta) \end{cases} \tag{31}$$

According to (18) and $i_{o1} + i_{o2} = 0$, the zero sequence plane currents are set as:

$$\begin{cases} i_{o1} = i_d{}'(k_5 \cos\theta + (k_6 + 1) \sin\theta) + i_q{}'((k_7 + 1) \cos\theta + k_8 \sin\theta) \\ i_{o2}= -i_d{}'(k_5 \cos\theta + (k_6 + 1) \sin\theta) - i_q{}'((k_7 + 1) \cos\theta + k_8 \sin\theta) \end{cases} \tag{32}$$

Minimizing the maximum current amplitude of each phase, it is calculated that:

$$\begin{cases} k_1 = -0.02, k_2 = -0.88, k_3 = -0.75, k_4 = 0.3 \\ k_5 = -0.35, k_6 = -0.59, k_7 = -0.64, k_8 = 0.21 \end{cases}$$

Therefore, in field-oriented control $i_d{}' = 0$, the current of the harmonic plane and zero sequence plane should be given as follows:

$$\begin{cases} i_{z1} = 0.81 i_q \sin(\theta - 68.57^\circ) \\ i_{z2} = 0.674 i_q \sin(\theta - 71.94^\circ) \\ i_{o1} = 0.415 i_q \sin(\theta - 120.21^\circ) \\ i_{o2} = 0.415 i_q \sin(\theta + 59.79^\circ) \end{cases} \tag{33}$$

Similarly, the fault-tolerant control current in a two-phase or multi-phase open circuit fault can be calculated. We take a two-phase open circuit as an example, including 30°, 90°, 120° and 150°. For example, in an AB two-phase open circuit, the electric angle of two fault phases is 120°. In Structure 1, when taking MCC as the control objective in the field-oriented control $i_d{}' = 0$, the harmonic and zero sequence plane currents shall be given as follows according to the derivation process above:

$$\begin{cases} i_{z1} = i_q{}' \sin\theta \\ i_{z2} = i_q{}' \cos\theta \\ i_{o1} = i_{o2} = 0 \end{cases} \tag{34}$$

In Structure 2, taking MCC as the control objective in the field-oriented control $i_d{}' = 0$, the harmonic and zero sequence plane current components calculated should be given as:

$$\begin{cases} i_{z1} = 0.721 i_q{}' \sin(\theta - 13.88^\circ) \\ i_{z2} = 0.916 i_q{}' \sin(\theta + 100.88^\circ) \\ i_{o1} = 0.346 i_q{}' \sin(\theta + 29.97^\circ) \\ i_{o2} = 0.346 i_q{}' \sin(\theta - 150.03^\circ) \end{cases} \tag{35}$$

When taking MTO as the control objective in field-oriented control, the harmonic and zero sequence plane current components are given as follows:

$$\begin{cases} i_{z1} = i_q{}' \sin\theta \\ i_{z2} = i_q{}' \cos\theta \\ i_{o1} = i_{o2} = 0 \end{cases} \tag{36}$$

We compare the stator copper loss and maximum current of two structures with MCC and MTO with single-phase and two-phase open circuits in field-oriented control, as shown in Table 1.

Table 1. Fault-tolerant control of DTP-PMSM in single-phase and two-phase open circuits with two current optimization objectives.

	MCC				MTO			
Fault phase	Structure 1		Structure 2		Structure 1		Structure 2	
	Loss	Imax	Loss	Imax	Loss	Imax	Loss	Imax
A	$9i_q'^2R_s$	$1.8i_q'$	$8i_q'^2R_s$	$1.85i_q'$	$12i_q'^2R_s$	$1.73i_q'$	$10.4i_q'^2R_s$	$1.44i_q'$
A,D (30°)	$48i_q'^2R_s$	$3.46i_q'$	$47.9i_q'^2R_s$	$3.5i_q'$	$48i_q'^2R_s$	$3.46i_q'$	$48i_q'^2R_s$	$3.46i_q'$
A,F (90°)	$12i_q'^2R_s$	$1.73i_q'$	$10.5i_q'^2R_s$	$1.9i_q'$	$12i_q'^2R_s$	$1.73i_q'$	$12i_q'^2R_s$	$1.73i_q'$
A,B (120°)	$12i_q'^2R_s$	$2i_q'$	$10i_q'^2R_s$	$2.03i_q'$	$60i_q'^2R_s$	$6i_q'$	$16.8i_q'^2R_s$	$2.27i_q'$
A,E (150°)	$48i_q'^2R_s$	$3.46i_q'$	$11.2i_q'^2R_s$	$2.07i_q'$	$48i_q'^2R_s$	$3.46i_q'$	$12.9i_q'^2R_s$	$1.79i_q'$

It can be seen from the table that the postfault stator copper losses in Structure 1 and Structure 2 are different. The stator copper consumption in a fault-tolerant single-phase open circuit will be less than that in a two-phase open circuit. Similarly, copper consumption in a fault-tolerant three-phase and multi-phase open circuit will be greater. When the electric angle of two fault phases is 30°or 150°, both the copper consumption and maximum phase current are very large no matter whether the control objective is

MCC or MTO. It can be seen that in Structure 1, when taking MTO as the control target, the copper consumption of the stator is large when taking MTO as the control target. Therefore, we need to take some measures to avoid the above faults as far as possible in the actual operation.

5. Motor Torque Analysis

In this paper, DTP-PMSM with a neutral point isolation connection method is adopted. In the field-oriented control system $i_d{}'= 0$, if the copper loss is minimized, $i_{z1} = i_{z2} = i_{o1} = i_{o2} = 0$. Each phase current is obtained through the inverse matrix of (5):

$$\begin{cases} i_A = -i_q{}' \sin(\omega t) \\ i_B = -i_q{}' \sin(\omega t - 120^\circ) \\ i_C = -i_q{}' \sin(\omega t + 120^\circ) \\ i_D = -i_q{}' \sin(\omega t - 30^\circ) \\ i_E = -i_q{}' \sin(\omega t - 150^\circ) \\ i_F = -i_q{}' \sin(\omega t + 90^\circ) \end{cases} \tag{37}$$

Comparing (9) and (37), the phase current amplitude is:

$$I_m = i_q{}' \tag{38}$$

The electromagnetic torque can be considered as the interaction of the rotating magnetomotive force generated by the winding current. The harmonic magnetic potential is ignored. When the dual three-phase motor is operating normally, the total stator magnetic potential is:

$$\begin{aligned} F_{6s} &= N_A i_A + N_B i_B + N_C i_C + N_D i_D + N_E i_E + N_F i_f \\ &= K[i_A \cos\alpha + i_B \cos(\alpha - 120^\circ) + i_C \cos(\alpha + 120^\circ) \\ &\quad + i_D \cos(\alpha - 30^\circ) + i_E \cos(\alpha - 150^\circ) + i_F \cos(\alpha + 90^\circ)] \end{aligned} \tag{39}$$

Ni (i = A, B, C, D, E,F) represents the winding function. K is the magnetic potential factor, and α is the electrical angle of the winding space. Substituting (9) and (38) into (39), we obtain:

$$F_{6s} = 3Ki_q{}' \sin(\alpha - \omega t) \tag{40}$$

Since Ψ_f and i_d are in the same direction, the electromagnetic torque expression is:

$$T_e = F_{6s} \cdot \psi_f = 3Ki_q{}'\psi_f \sin(90^\circ) = 3Ki_q{}'\psi_f \tag{41}$$

It can be seen that the torque of DTP-PMSM only contains DC in normal operation.

When one phase open circuit occurs, taking the F-phase open circuit as an example, the total magnetic potential of the remaining five-phase windings of the DTP-PMSM is:

$$\begin{aligned} F_{5s} &= N_A i_A + N_B i_B + N_C i_C + N_D i_D + N_E i_E \\ &= K[i_A \cos\alpha + i_B \cos(\alpha - 120^\circ) + i_C \cos(\alpha + 120^\circ) + i_D \cos(\alpha - 30^\circ) + i_E \cos(\alpha - 150^\circ)] \end{aligned} \tag{42}$$

Substituting (9) and (38), we obtain:

$$F_{5s} = \frac{1}{2}Ki_q{}'[5\sin(\alpha - \omega t) - \sin(\alpha + \omega t)] \tag{43}$$

It can be seen that the magnetic potential of DTP-PMSM contains a positive sequence component and a negative sequence component when one phase is open. The torque is:

$$T_{e1} = F_{5s} \cdot \psi_f = \frac{1}{2}Ki_q{}'\psi_f[5 - \sin(2\omega t)] \tag{44}$$

It can be seen that the torque with one phase open contains a DC component and a second harmonic component.

When MCC is taken as the fault-tolerant control target, (22) is transformed through the inverse matrix of (5) to obtain each phase current as:

$$\begin{cases} i_A{}' = -i_q{}' \sin \omega t \\ i_B{}' = 1.803 i_q{}' \sin(\omega t + 73.9^\circ) \\ i_C{}' = 1.803 i_q{}' \sin(\omega t - 73.9^\circ) \\ i_D{}' = -0.866 i_q{}' \sin \omega t \\ i_E{}' = -0.866 i_q{}' \sin \omega t \\ i_F{}' = 0 \end{cases} \tag{45}$$

Therefore, the magnetic potential of DTP-PMSM is:

$$F_{5s}{}' = N_A i_A{}' + N_B i_B{}' + N_C i_C{}' + N_D i_D{}' + N_E i_E{}' = 3K i_q{}' \sin(\alpha - \omega t) \tag{46}$$

The electromagnetic torque is:

$$T_{e1}{}' = F_{5s}{}' \cdot \psi_f = \frac{3}{2} N i_q{}' \psi_f \sin(90^\circ) = 3K i_q{}' \psi_f \tag{47}$$

When MTO is set as the control target, through (28) and the inverse matrix of (5), the current of each phase is obtained as:

$$\begin{cases} i_{A1} = 0 \\ i_{B1} = \sqrt{3} i_q{}' \cos(\omega t) \\ i_{C1} = -\sqrt{3} i_q{}' \cos(\omega t) \\ i_{D1} = -\sqrt{3} i_q{}' \sin(\omega t) \\ i_{E1} = \sqrt{3} i_q{}' \sin(\omega t) \\ i_{F1} = 0 \end{cases} \tag{48}$$

Therefore, the magnetic potential of DTP-PMSM is:

$$F_{5s}{}'' = N_A i_{A1} + N_B i_{B1} + N_C i_{C1} + N_D i_{D1} + N_E i_{E1} = 3K i_q{}' \sin(\alpha - \omega t) \tag{49}$$

And then the electromagnetic torque is:

$$T_{e1}{}'' = F_{5s}{}'' \cdot \psi_f = \frac{3}{2} N i_q \psi_f \sin(90^\circ) = 3K i_q{}' \psi_f \tag{50}$$

From (47) and (50), it can be seen that it effectively suppresses the second harmonic component in the torque with fault-tolerant control.

6. Simulation Analysis and Experimental Results

6.1. Simulation Analysis

The motor parameters are shown in Table 2. The DTP-PMSM neutral is isolated. The control system of DTP-PMSM is shown in Figure 3.

Table 2. Parameters of DTP-PMSM.

Parameter	Value
Rated power	1.5 kw
Rated current	6 A
Motor stator resistance	0.72 Ω
d-axis inductance L_d	1.65 mH
q-axis inductance L_q	1.65 mH
Flux linkage	0.13 Wb
Pole pairs	3
Rated speed n	2000 r/min

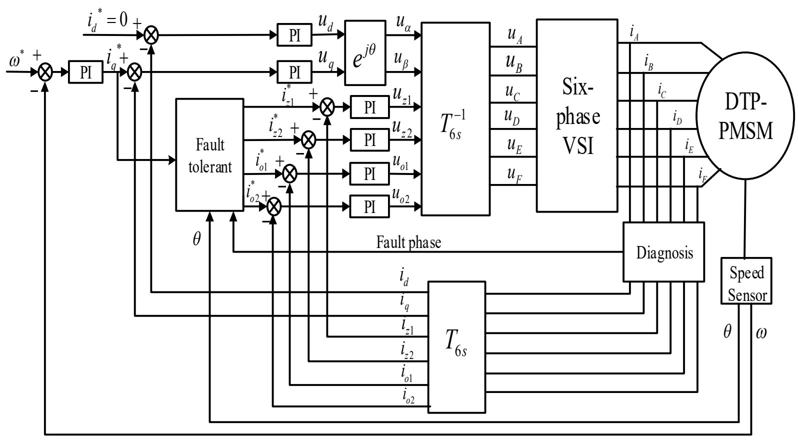

Figure 3. Control system of DTP-PMSM.

Figure 4a shows the current trajectory curve in α-β subspace. It is approximately circular when the motor operates healthily, which is consistent with (10). In the open circuit fault state, the current trajectory is no longer circular, as shown in Figure 4b.

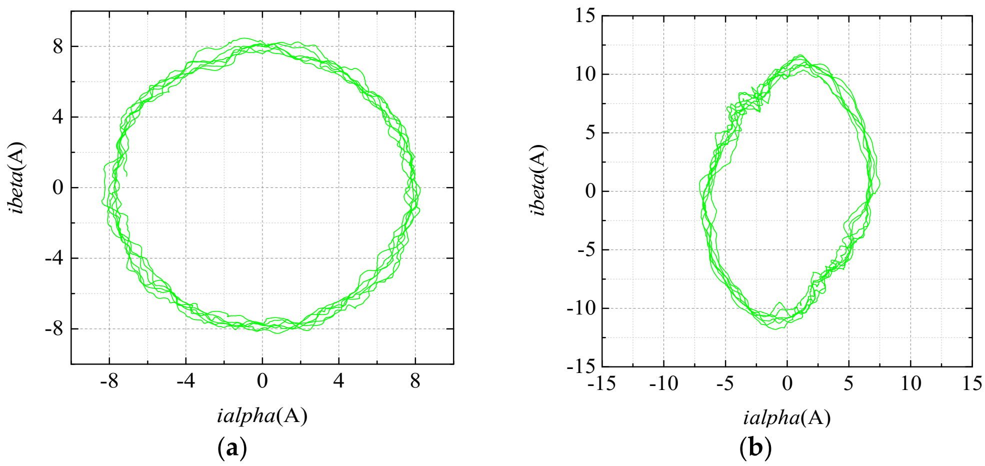

Figure 4. α-β subspace current trajectory. (**a**) Healthy motor. (**b**) F-phase open circuit.

Figure 5 shows the dq subspace current of a healthy state and an open circuit fault state. It can be seen that the dq current of the motor is no longer stable in the open circuit fault, and the oscillation is severe.

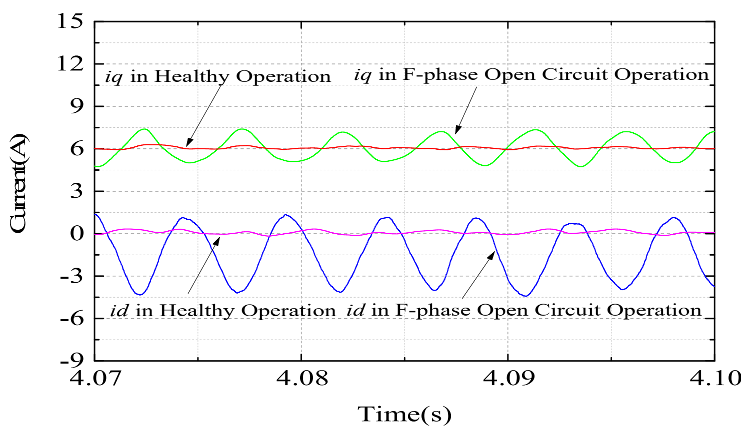

Figure 5. Motor healthy and F-phase open circuit dq current.

Figure 6 shows the torque waveform of a motor without a fault and with an F-phase open circuit. The motor rated torque is 7.1 Nm. It can be seen that motor torque ripple is obvious with an open circuit fault, which will produce a lot of noise.

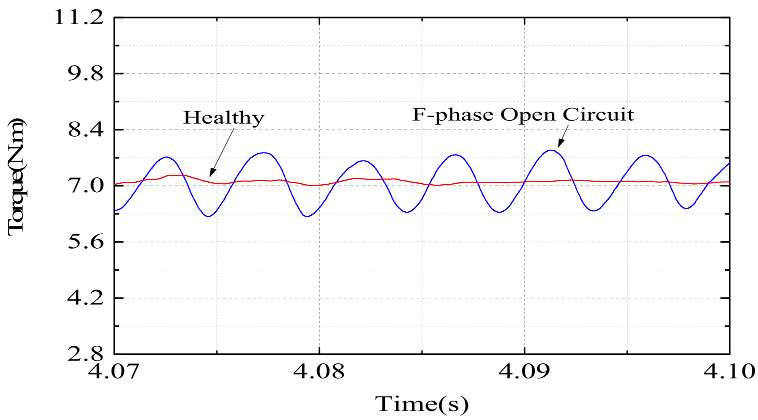

Figure 6. Torque of the motor in healthy and open circuit operation.

Figure 7 shows the speed waveform of the motor in healthy operation and F-phase open circuit operation. It can be seen that motor speed is stable at the given speed when there is no fault. While the speed fluctuates greatly with an open circuit fault, it cannot run smoothly.

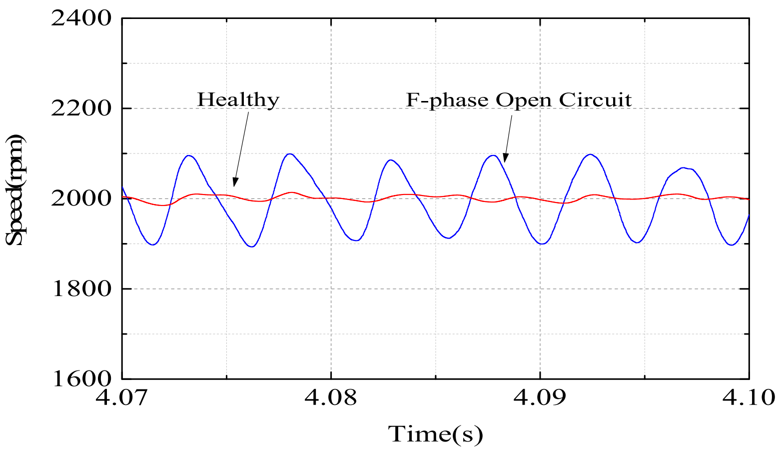

Figure 7. Motor speed in healthy operation and open circuit operation.

Figure 8 shows the speed of the motor in open circuit fault and fault-tolerant operation. It can be seen that motor has large speed oscillation and poor speed regulation performance in open circuit fault, and the speed ripple is as high as 10%. The speed ripple is smaller with the proposed MCC and MTO than that with traditional MCC and MTO. The motor speed ripple is reduced to 2.3% with the control strategy of the proposed MCC based on MPC. The motor speed ripple is reduced to 2.5% with the control strategy of the proposed MTO based on MPC.

Figure 9 shows the speed THD of the motor at different speeds without fault tolerance, traditional MCC and MTO with fault tolerance, and the MCC and MTO with fault tolerance based on MPC proposed in this paper. THD is significantly lower with fault-tolerant control than that without fault-tolerant control. Moreover, compared with the traditional MCC and MTO, the THD weakening effect is better with the proposed MCC and MTO.

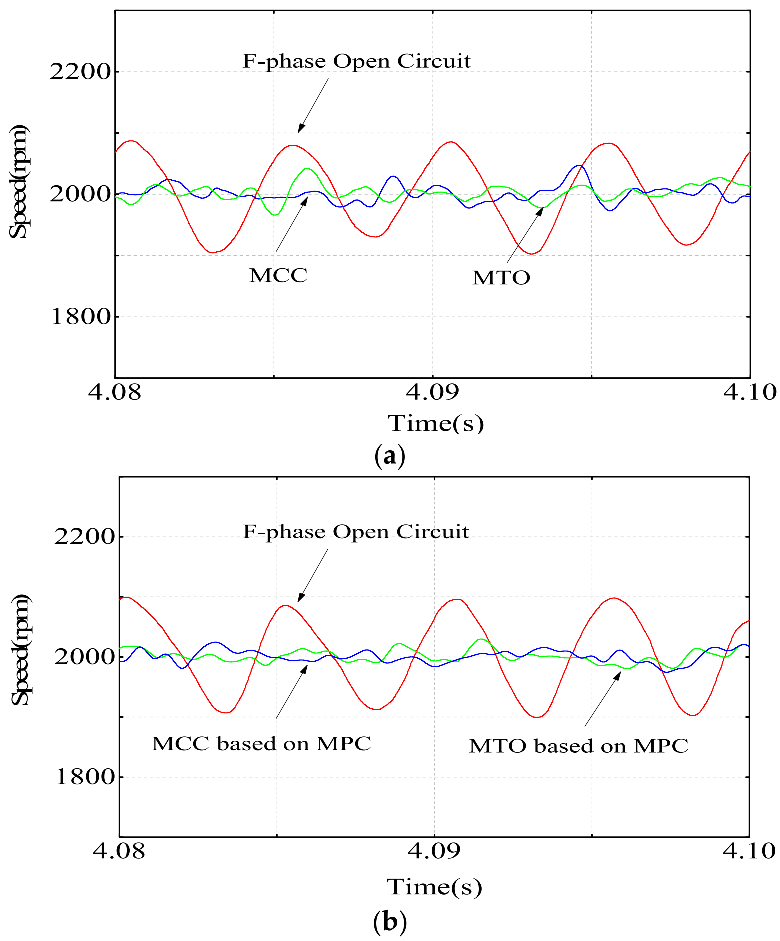

Figure 8. Speed of motor in fault operation and fault-tolerant control. (**a**) Fault-tolerant control with traditional MCC and MTO. (**b**) Fault-tolerant control with proposed MCC and MTO.

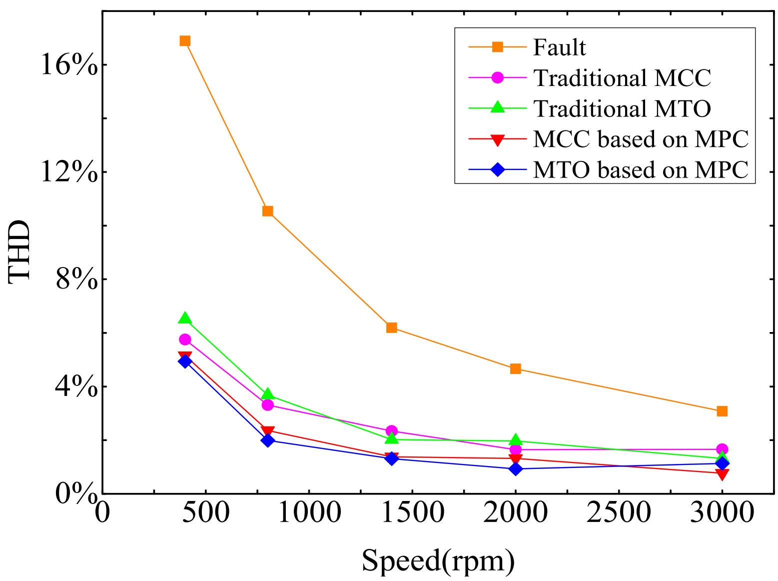

Figure 9. THD of motor speed.

Figure 10 shows the torque waveform comparison between open circuit fault operation and fault-tolerant operation. It can be seen that the torque ripple is obvious without fault-tolerant control, which will produce large noise. However, the torque fluctuation is basically stable and small with the two fault-tolerant controls. The THD analysis of torque with fault operation and two fault-tolerant control strategies is shown in Figure 11. The result shows that the THD of the torque weakening effect is better with the proposed MCC and MTO than that with the traditional method. Then, the harmonic analysis of the torque with the proposed fault-tolerant control method is carried out as shown in Figure 12. The result shows that the second harmonic components of the torque in fault operation is very high, and is significantly reduced through the proposed fault-tolerant control. This is consistent with the analysis in Section 5.

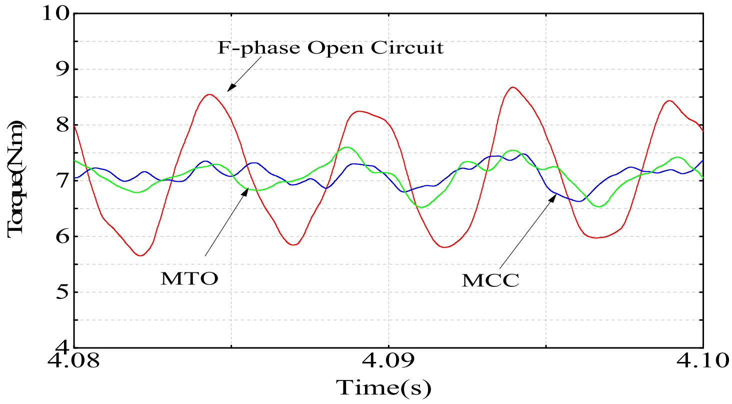

(**a**)

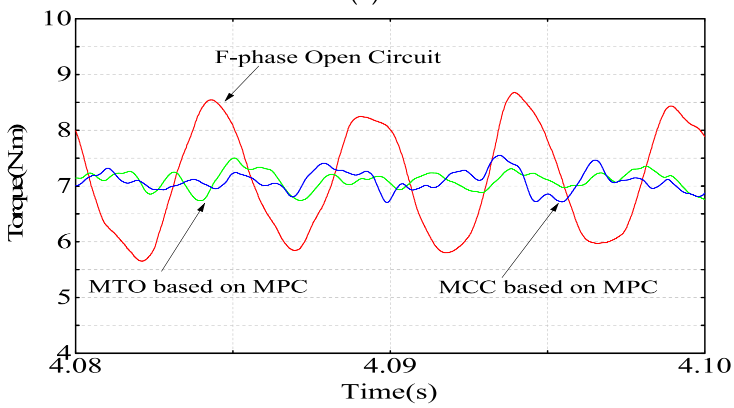

(**b**)

Figure 10. Torque in fault operation and fault-tolerant operation. (**a**) Fault-tolerant control with traditional MCC and MTO. (**b**) Fault-tolerant control with proposed MCC and MTO.

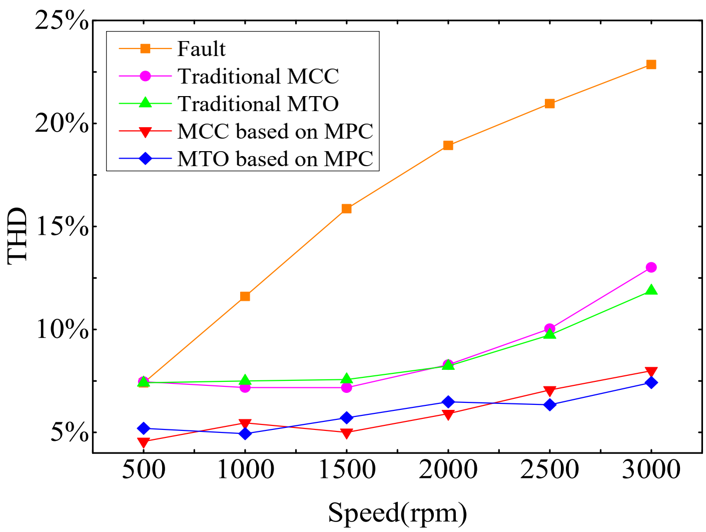

Figure 11. THD of motor torque.

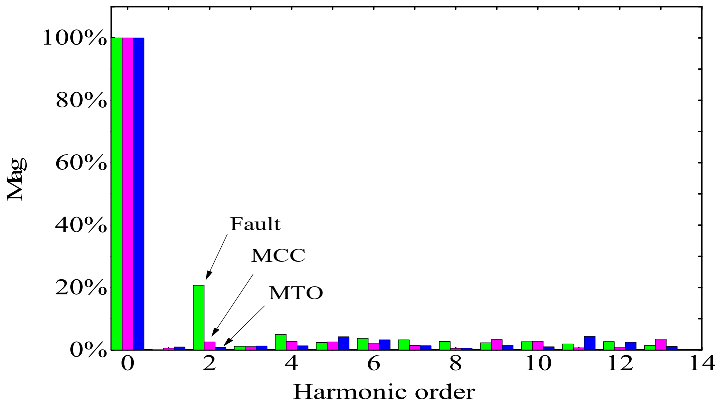

Figure 12. Torque FFT analysis.

Figure 13 shows the current during the healthy operating, F-phase open circuit and fault-tolerant control state. The amplitude and phase of the remaining phase current can be reasonably arranged through fault-tolerant control. It can be seen from the figure that the distortion of the current waveform is small when the proposed MCC and MPC methods are adopted.

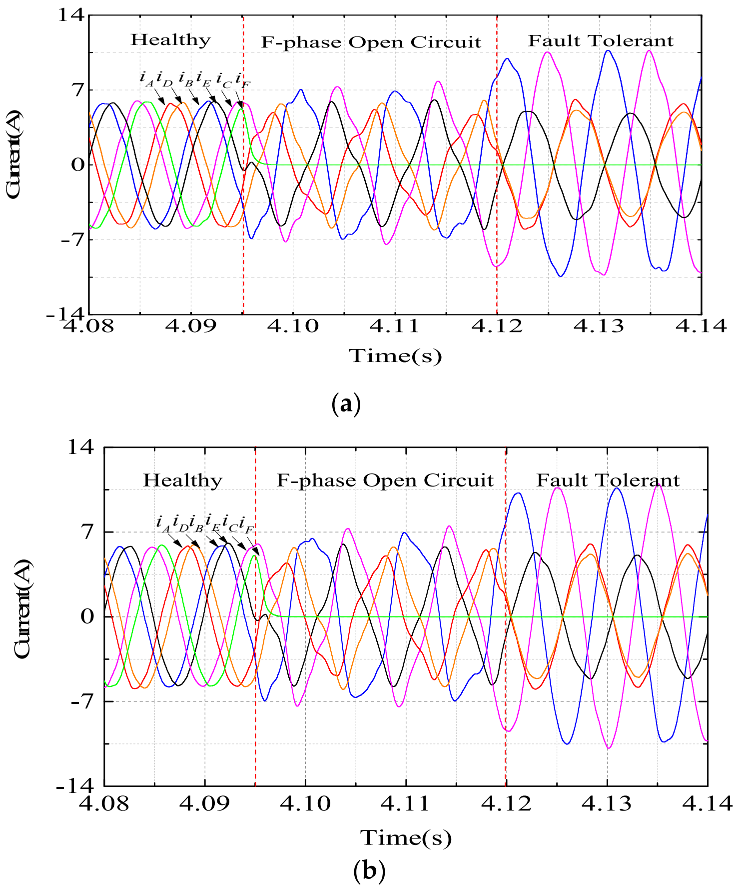

Figure 13. *Cont.*

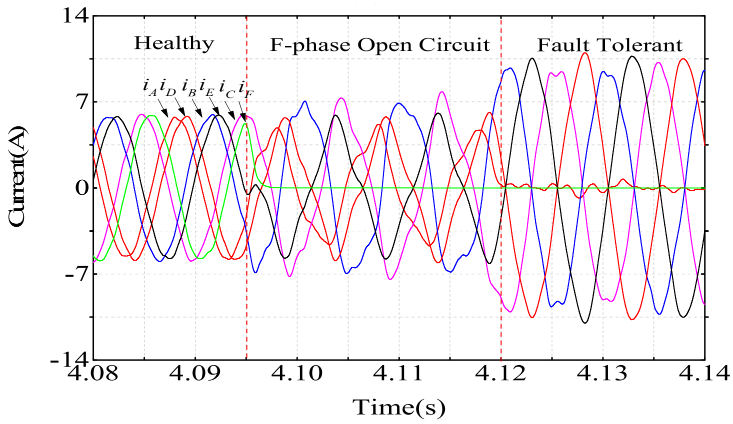

(**c**)

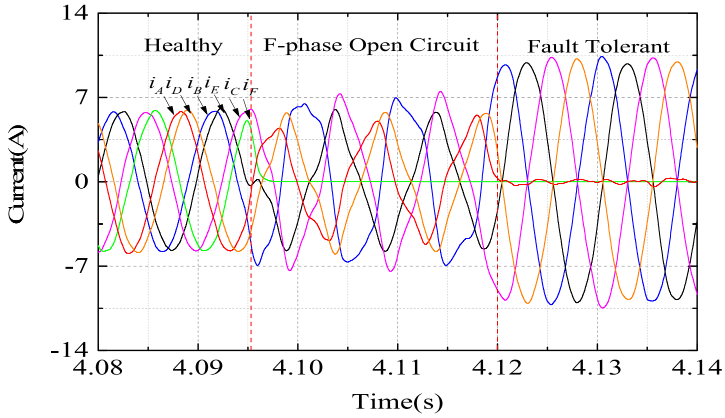

(**d**)

Figure 13. Motor healthy, fault and fault-tolerant currents. (**a**) Fault-tolerant control with optimal objective of the traditional MCC. (**b**) Fault-tolerant control with optimal objective of the proposed MCC. (**c**) Fault-tolerant control with optimal objective of the traditional MTO. (**d**) Fault-tolerant control with optimal objective of the proposed MTO.

Figure 14 compares the dq current in open circuit fault operation and fault-tolerant control operation. It can be seen from the figure that dq current oscillation is obviously unstable in the open circuit fault. When the proposed fault-tolerant control is adopted, the dq current can be effectively stabilized at a given value. It can achieve better vector control and ensure reliable operation of the motor.

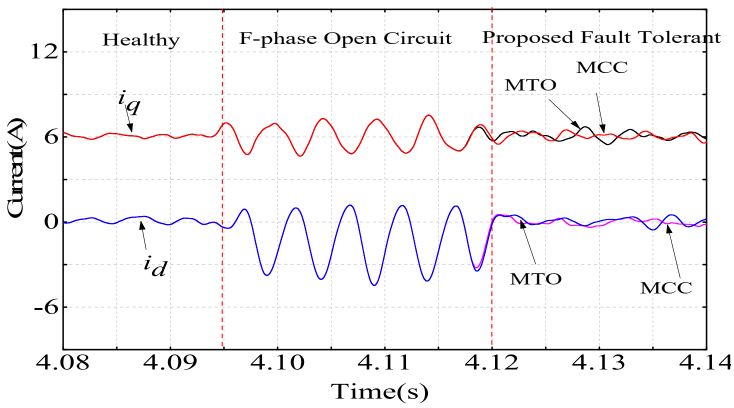

Figure 14. *d*-*q* current in fault and the proposed fault-tolerant control operation.

6.2. Experiment Results

A DTP-PMSM experimental platform was built to verify the effectiveness of the strategy proposed in this paper. The experimental platform is shown in Figure 15. The main controller adopts DSP chip TMS32028335.

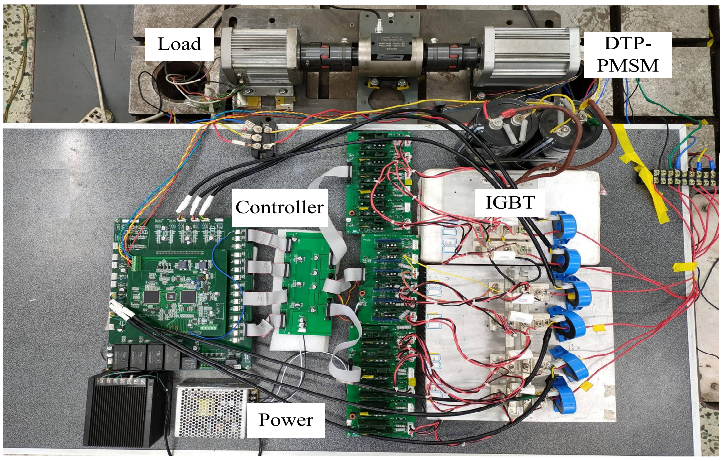

Figure 15. DTP-PMSM experimental platform.

For when the F-phase was open, the measured phase current, speed waveform and fault characteristic value curve are shown in Figure 16. It can be seen that when the fault occurred, the current of the non-fault phase increased and was no longer sinusoidal. The waveform of the speed pulsated obviously. The characteristic value of the fault phase reached 0.64, which is consistent with the theoretical analysis.

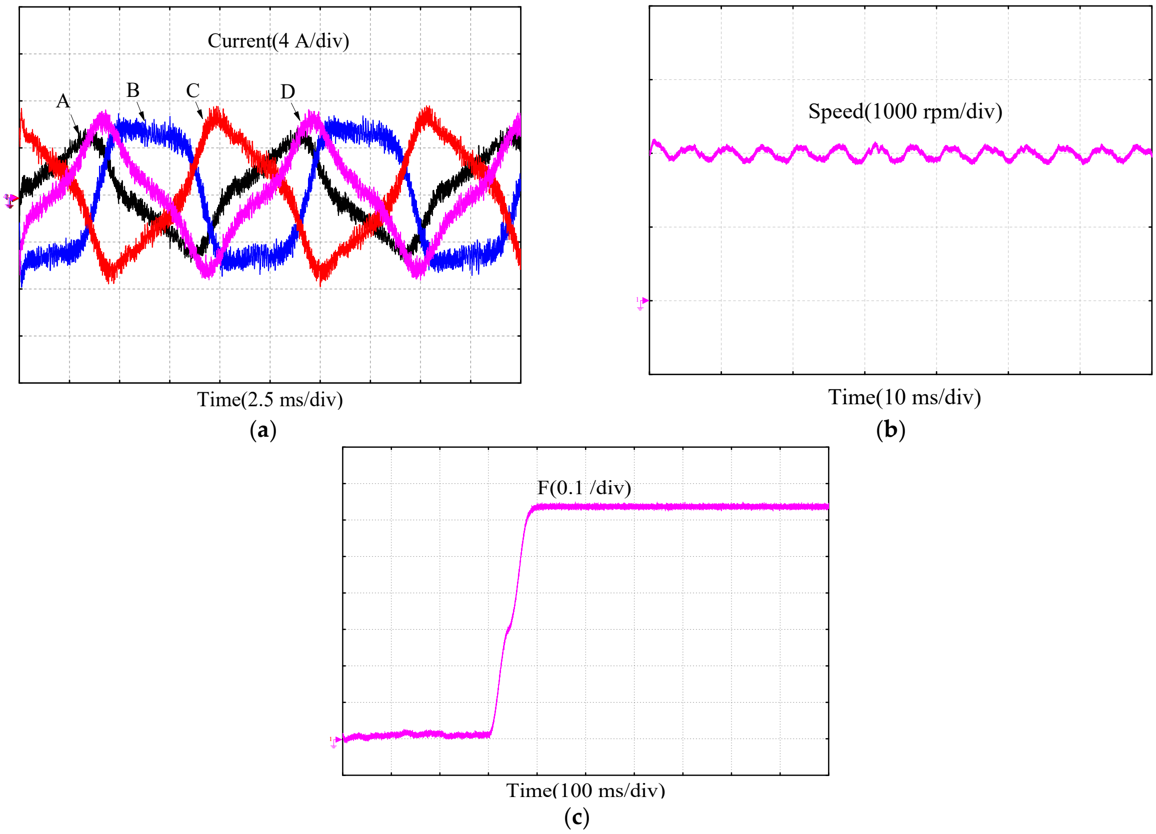

Figure 16. Motor waveform during F-phase open circuit fault. (**a**) Current waveform. (**b**) Speed waveform. (**c**) Fault characteristic value.

The measured current and speed waveforms after putting in the traditional fault-tolerant control strategy are shown in Figure 17. The response of the proposed fault-tolerant control is shown in Figure 18. The results show that the proposed control strategy had a better fault tolerance effect and effectively reduced distortion.

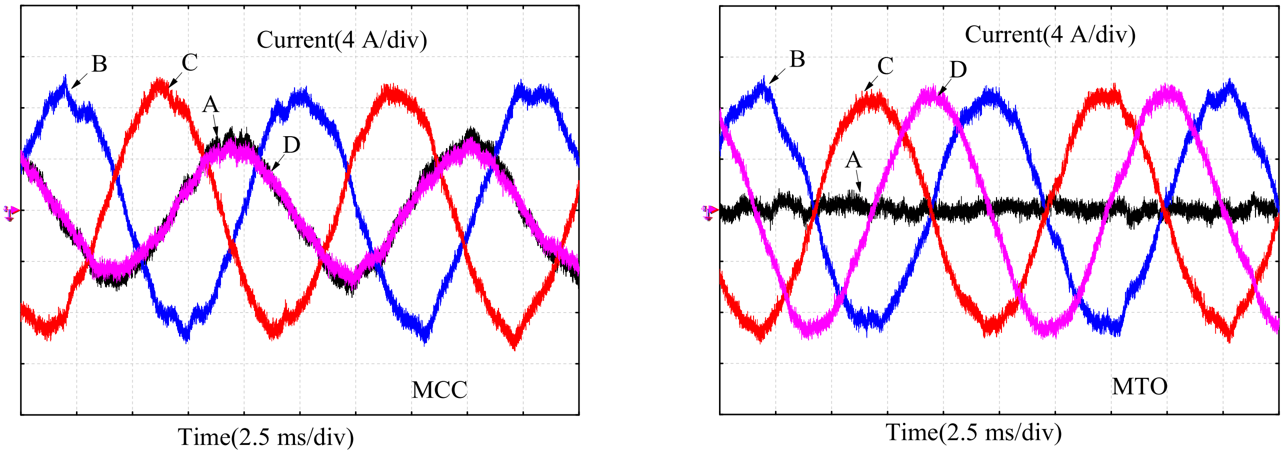

(**a**)

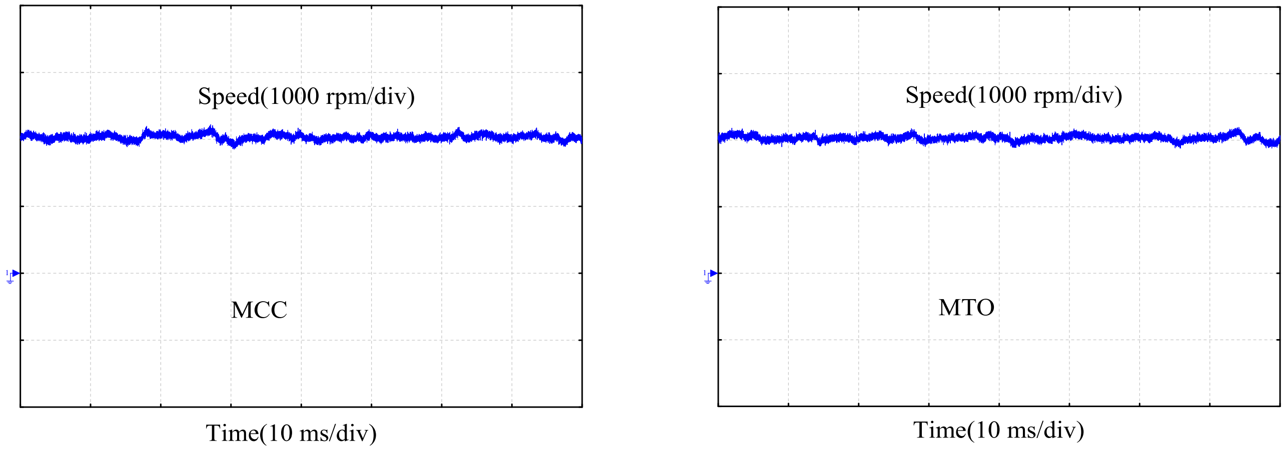

(**b**)

Figure 17. Motor waveform with traditional MCC and MTO. (**a**) Current waveform. (**b**) Speed waveform.

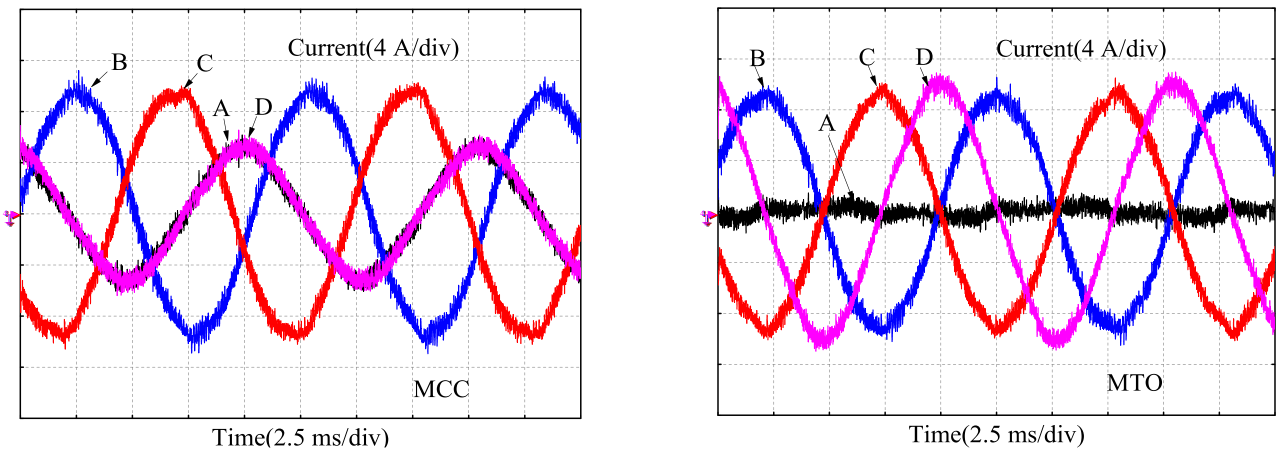

(**a**)

Figure 18. *Cont*.

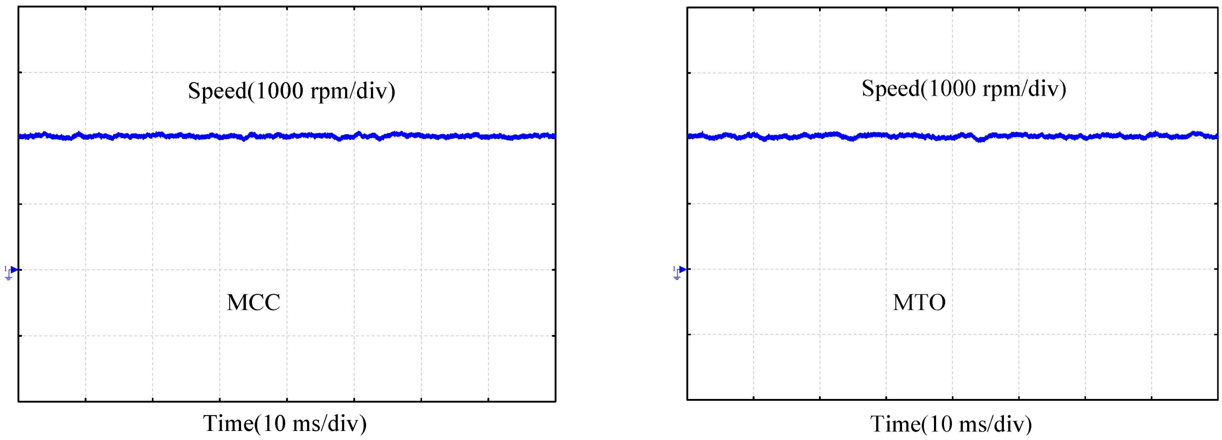

(**b**)

Figure 18. Motor waveform with fault-tolerant control. (**a**) Current waveform. (**b**) Speed waveform.

7. Conclusions

In this paper, a high-performance fault-tolerant control strategy with model prediction is proposed to reduce the total harmonic distortion of DTP-PMSM drives. The contributions of the study are concluded as following.

(a) In the study, an open circuit fault diagnosis method based on a normalized current was applied to diagnose the fault phase in order to carry out the corresponding fault-tolerant control strategy.

(b) A novel fault-tolerant control strategy based on MPC was proposed for the purpose of reducing the harmonic distortion and improving fault tolerance performance. It adjusts the current setting of z_1-z_2 and o_1-o_2 subspace without changing the mathematical model of the motor. The fault-tolerant control strategy is studied by taking the proposed MCC and MTO as the optimization objectives.

The simulation and experimental results show that the proposed fault-tolerant control strategy can effectively improve the fault tolerance performance and reduce harmonic distortion. This ensures the stable operation and good performance of DTP-PMSM when an open circuit fault occurs.

Author Contributions: Conceptualization, L.Z. and H.G.; data curation, L.Z.; funding acquisition, B.G. and D.T.; Investigation, B.G.; Methodology, L.Z.; project administration, B.G.; resources, H.G.; Software, L.Z.; Supervision, H.G.; validation, L.Z.; writing—original draft, L.Z.; writing—review & editing, H.G. and D.T. All authors have read and agreed to the published version of the manuscript.

Funding: This research was funded by National Basic Research Program of China (JCKY2018412C006).

Conflicts of Interest: The authors declare no conflict of interest.

References

1. Jia, S.; Liu, Z.; Liang, D. Review of fault tolerant control strategies for multiphase motors [J/OL]. *J. Xi'an Jiaotong Univ.* **2021**, *6*, 1–9.
2. Chen, B.; Lv, J.; Jiang, X. Simplified Model Predictive Control of a Twelve-Phase Permanent Magnet Synchronous Motor. In Proceedings of the IECON 2019—45th Annual Conference of the IEEE Industrial Electronics Society, Lisbon, Portugal, 19 April 2019; pp. 1345–1350.
3. Xu, J.; Zhang, B.; Fang, H.; Guo, H. Guaranteeing the fault transient performance of aerospace multiphase permanent magnet motor system: An adaptive robust speed control approach. *CES Trans. Electr. Mach. Syst.* **2020**, *4*, 114–122. [CrossRef]
4. Barrero, F.; Duran, M.J. Recent advances in the design, modeling and control of multiphase machines—Part 1. *IEEE Trans. Ind. Electron.* **2016**, *63*, 449–458. [CrossRef]
5. Feng, G.; Lai, C.; Li, W.; Tjong, J.; Kar, N.C. Open-Phase Fault Modeling and Optimized Fault-Tolerant Control of Dual Three-Phase Permanent Magnet Synchronous Machines. *IEEE Trans. Power Electron.* **2016**, *34*, 11116–11127. [CrossRef]
6. Zheng, L.; Yang, O.; Lin, H.; Chao, M.; Siguo, Z. Vector control system of multi-level double y-shift 30° permanent magnet synchronous motor. *Acta Electrotech. Sin.* **2016**, *31*, 45–56.

7. Ma, X.; Zheng, A.; Zhang, H.; Liu, L. Sliding mode variable structure control technology for double y-shift 30° six phase PMSM. *J. Electr. Mach. Control* **2018**, *22*, 1292.
8. Gaeta, A.; Scelba, G.; Consoli, A. Modeling and control of three-phase PMSMs under open-phase fault. *IEEE Trans. Ind. Appl.* **2013**, *49*, 74–83. [CrossRef]
9. Gao, C.; Zhao, W.; Ji, J.; Chen, Q. Low harmonic double three phase permanent magnet synchronous motor and its fault tolerant control. *Acta Electrotech. Sin.* **2017**, *32*, 124–130.
10. Hosseyni, A.; Trabelsi, R.; Mimouni, M.F.; Iqbal, A. Fault tolerant control strategy of a five-phase permanent magnet synchronous motor drive. In Proceedings of the 16th International Conference on Sciences and Techniques of Automatic Control and Computer Engineering (STA), Monastir, Tunisia, 19 April 2015; pp. 218–222.
11. Wang, S.; Chen, R.; Lee, F.C.; van Wyk, J.D. Improved passive filter configurations for high-frequency conducted EMI in power electronics. In Proceedings of the IEEE European Power Electronics, Dresden, Germany, 11–14 September 2005.
12. Liu, H.T.; Fu, R.J.; Lipo, A.T. A strategy for improving reliability of fifield-oriented controlled induction motor drives. *IEEE Trans. Ind. Appl.* **1993**, *29*, 910–918.
13. Fu, R.J.; Lipo, A.T. Disturbance-free operation of a multiphase current-regulated motor drive with an open phase. *IEEE Trans. Ind. Appl.* **1994**, *30*, 1267–1274.
14. Yao, G.; Yin, Z.; Zhou, L.; Wang, J. Fault tolerant control of six phase permanent magnet synchronous generator. *J. Electr. Mach. Control* **2018**, *22*, 1–10.
15. Gao, H.; Yang, G. Modeling and control of five phase permanent magnet synchronous motor in open phase operation. *Acta Electrotech. Sin.* **2016**, *31*, 93–101.
16. Yang, Z. *Research on Fault Tolerant Control Strategy of Dual Three Phase Permanent Magnet Synchronous Motor*; Harbin Institute of Technology: Harbin, China, 2018.
17. Zhou, C.; Tang, W.; Sun, X.; Zhou, Z.; Yang, G.; Su, J. Control strategy for dual three-phase PMSM based on reduced order mathematical model under fault condition due to open phases. *J. Eng.* **2018**, *2018*, 489–494.
18. Zhao, M.; Quan, L.; Zhang, C.; Zhu, X. Single phase open circuit fault decoupling fault tolerant control of five phase permanent magnet synchronous motor based on minimum copper consumption. *Appl. Mot. Control* **2017**, *44*, 126–133.
19. Yang, J.; Li, T.; Yang, G. Modeling and control of one phase open circuit double three phase permanent magnet synchronous motor. *Acta Electrotech. Sin.* **2011**, *26*, 5862–5872.
20. Giangrande, P.; Madonna, V.; Nuzzo, S.; Spagnolo, C.; Gerada, C.; Galea, M. Reduced Order Lumped Parameter Thermal Network for Dual Three-Phase Permanent Magnet Machines. In Proceedings of the 2019 IEEE Workshop on Electrical Machines Design, Control and Diagnosis (WEMDCD), Athens, Greece, 22–23 April 2019; pp. 71–76.
21. Zhang, W.; Xu, Y.; Chen, B. Control of Dual Three-Phase Permanent Magnet Synchronous Motor under Open Phase Fault Conditions. In Proceedings of the 2016 IEEE Vehicle Power and Propulsion Conference (VPPC), Hangzhou, China, 11 December 2016; pp. 1–5.
22. Zhao, Y.; Lipo, T.A. Modeling and control of a multi-phase induction machine with structural unbalance. *IEEE Trans. Energy Convers.* **1996**, *11*, 570–577. [CrossRef]
23. Ryu, M.H.; Kim, W.J.; Sul, K.S. Synchronous-frame current control of multiphase synchronous motor under asymmetric fault condition due to open phases. *IEEE Trans. Ind. Appl.* **2006**, *42*, 1062–1070.
24. Tian, D.; Chen, L.; Hou, L.J.; Pan, J. Modeling and simulation of dual three-phase induction machine with two opened phases. In Proceedings of the IEEE International Conference on Industrial Technology, Chengdu, China, 21–24 April 2008; pp. 1–5.
25. Tiao, S.; Zhou, M.; Ouyang, H.L.; Liu, L. Vector control of multiphase PMSM with asymmetric structure. *Trans. China Electrotech. Soc.* **2004**, *19*, 37–41.
26. Wang, W.; Zhang, J.; Cheng, M.; Li, S. Fault-Tolerant Control of Dual Three-Phase Permanent-Magnet Synchronous Machine Drives Under Open-Phase Faults. *IEEE Trans. Power Electron.* **2016**, *32*, 2052–2063. [CrossRef]
27. Fan, Y. *Research on Control Strategy of Five Phase Permanent Magnet Synchronous Motor Based on Third Harmonic Injection*; Harbin Institute of Technology: Harbin, China, 2016.
28. Feng, G.; Lai, C.; Kelly, M.; Kar, N.C. Dual Three-Phase PMSM Torque Modeling and Maximum Torque per Peak Current Control Through Optimized Harmonic Current Injection. *IEEE Trans. Ind. Electron.* **2018**, *66*, 3356–3368. [CrossRef]
29. Zhou, C.; Yang, G.; Su, J.; Sun, G. Open phase fault tolerant control strategy of dual three phase permanent magnet synchronous motor based on normal decoupling transformation. *Acta Electrotech. Sin.* **2017**, *32*, 86–96.
30. Locment, F.; Semail, E.; Kestelyn, X. Vectorial approach-based control of a seven-phase axial flflux machine designed for fault operation. *IEEE Trans. Ind. Electron.* **2008**, *55*, 3682–3691. [CrossRef]
31. Tani, A.; Mengoni, M.; Zarri, L.; Serra, G.; Casadei, D. Control of multiphase induction motors with an odd number of phases under opencircuit phase faults. *IEEE Trans. Power Electron.* **2012**, *27*, 565–577. [CrossRef]
32. Akay, A.; Lefley, P.; Kansara, M. Open-Circuit Fault-Tolerant Control for a Five-Phase Permanent Magnet Synchronous Machine Drive. In Proceedings of the 2020 7th International Conference on Electrical and Electronics Engineering (ICEEE), Antalya, Turkey, 14–16 April 2020; pp. 150–154.
33. Yu, Y. *Research on Control Technology of Double y-Shift 30° Six Phase Permanent Magnet Synchronous Motor*; Harbin Institute of Technology: Harbin, China, 2015.